Parabolic Mirror Focusing of Spatiotemporally Coupled Ultrashort Terahertz Pulses

Haoran Zhang, Cheng Li, Zixin Guo, Xiazhen Xu, Jingya Li, Biaobin Li, Zhigang He, Shancai Zhang, and Qika Jia

***Abstract*—Ultrashort terahertz (THz) beam is often affected by spatio-temporal distortion due to its long wavelength, and this spatio-temporal coupling will degrade the focusing effect. Here, we develop a numerical model for calculating the vector focusing of ultrashort pulses with arbitrary spatial and temporal distribution, which adopt the vector diffraction integral and coherent spectrum superposition methods. Leveraging it, the focusing of a broadband pulse can be characterized together with its vector characteristics and we explore the influences of multifarious spatio-temporal couplings on the focusing of ultrashort THz pulses. In addition, the possibility of focusing the ultrashort THz radiation from an undulator to 1 GV/m is also discussed. This will provide further guidance for the non-equilibrium state of matter induced by ultrashort strong-field THz pulses.**

***Index Terms*—Parabolic mirror focusing, spatio-temporal coupling, ultrashort terahertz pulse, vector diffraction integral.**

I. Introduction

DUE to the low photon energy, terahertz (THz) radiation is an effective tool to study a large number of low-energy excitation phenomena. It can detect and control quasi-particle and collective excitation, and explore the rotation and vibration of molecular systems. Furthermore, the pursuit of ultrashort strong-field THz pulse is inspired by the realization of controllable operation of reaction and process, which can provide the necessary time resolution for the detection and control of the ultrafast dynamic process in material [1], [2]. The development of a single-cycle terahertz pulse source with a field strength of more than 1 MV/cm makes it possible to drive the new dynamic states of the materials. This field strength is equivalent to the intrinsic field strength of a wide range of strongly related materials, which will make the material present a property different from that in the equilibrium state. Specifically, the resonant excitation of the lattice structure and the non-resonant excitation of the charge carriers by the ultrashort strong-field THz pulse are utilized to promote the research on the dynamics of the coherent phonons [3], [4], [5], charge carriers [6], [7], [8], and spins [9], [10], [11], as well as the control of the molecular system [12], [13]. THz pulses can be utilized to the acceleration [14] and detection [15] of the electron beam, and the the electric field shape of the low-frequency THz pulses at the focus need to consider carefully in the case of direct electron acceleration [16]. Looking into the future, the field strength of 100 MV/cm may be applied to the studies on the coherent control of spin order of conductors, and the ultrashort THz transients with magnetic fields in the $1-10$ T ($3-30$ MV/cm) range can initiate magnetization reversal in metallic ferromagnetic samples [2].

In all these applications, focusing ultrashort THz radiation on the targeted materials is a very usual requirement. Optical focusing elements can be divided into reflective and transmissive types. The transmissive element in THz band has low transmission efficiency. Different from the transmissive optical elements, the parabolic mirror will not cause serious phase delay and absorption loss, so it is one of the commonly used components to build infrared and terahertz optics. When used to focus, it can not only effectively enhance the transient electric and magnetic field intensities but also focus the THz pulse into the specific space area. However, ultrashort pulses are often accompanied by spatio-temporal couplings (STCs) [17] which will affect the focus effect. The broad spectrum of ultrashort pulses increases the possibility of chromatic aberrations. Especially in the THz band, even without dispersive elements, there are non-negligible STCs due to its strong diffraction effect. Spatio-temporal couplings make the frequency components and phase distribution of ultrashort pulses different along spatial positions. Therefore, the focusing performance may be declined because of the dispersion behavior, where the focal spot size and pulse duration may be increased. Under the higher requirements of non-resonant control of matter on the electromagnetic field intensity, it is necessary to analyze the influence of STC on the focusing by a parabolic mirror. However, most of the existing researches on the spatial-temporal coupling of ultrashort THz pulse are directly measuring the spatio-temporal distribution after focusing, and there is a lack of characterization of the focusing process.

For the focusing process, especially in the case of tight focusing, the paraxial approximation is no longer applicable, and the vector effect of electromagnetic field becomes critical. Some analytical results provide the closed approximation results of the tightly focused field and are convenient to describe the spatio-temporal evolution of ultrashort pulses [18], [19]. However, its simplification of the incident field makes it difficult

Manuscript received 20 May 2023; revised 13 June 2023; accepted 15 June 2023. Date of publication 20 June 2023; date of current version 28 June 2023. This work was supported by the Youth Innovation Promotion Association of the Chinese Academy of Sciences. *(Corresponding author: Zhigang He.)*

The authors are with the National Synchrotron Radiation Laboratory, University of Science and Technology of China, Hefei 230029, China (e-mail: zhrzhm@ustc.edu.cn; lc199622@mail.ustc.edu.cn; gzixin@mail.ustc.edu.cn; xiazhenxu@mail.ustc.edu.cn; sa22231053@mail.ustc.edu.cn; biaobin@ustc.edu.cn; hezhg@ustc.edu.cn; shancai@ustc.edu.cn; jiaqk@ustc.edu.cn).

Digital Object Identifier 10.1109/JPHOT.2023.3287483

to consider the details of the electromagnetic field generated by the reflection of a given mirror geometry. The propagation equation can be used for the numerical realization of tight focusing with the vector effect [20], [21], [22]. Therein, Fedorov et al. [20] solved the vector problem by the scalar wave equation through the method of conversion optics, but only the intensity characteristics of the final electromagnetic field are retained. The method in [21], [22] solved the vector propagation equation under the tightly focused parabolic mirror through Hertz vector and non-paraxial input conditions and is called Unidirectional Hertz vector Propagation Equation. However, the propagation equation has not been used to solve the case of an ultrashort pulse yet, and the numerical realization of the propagation equation requires a lot of calculation consumption to solve the vector equation in the whole propagation space.

The vector diffraction integral (VDI) method can directly obtain the electromagnetic field distribution of the targeted focal plane. The rigorous vector diffraction theory of tight focusing problem began with Ignatowski's solution of Maxwell's equations under certain boundary conditions in cylindrical coordinates [23]. Then, Stratton and Chu [24] expressed the reflection problem as a vector integral equation using Green's theorem. In addition, Richards and Wolf [25], [26] constructed another different integral equation. Stratton-Chu's vector diffraction integral is widely used to study the tight focusing of parabolic mirrors [27], [28], [29], [30] and is further combined with the coherent superposition of monochromatic fields to deal with the focusing of ultrashort broadband pulses [31], [32]. However, these studies assume an ultrashort pulse with a plane wavefront, and there is no discussion about the focusing together with spatio-temporal couplings.

In this paper, we explore the effect of STCs on the focusing of ultrashort pulses by vector diffraction integral-based method. For a linearly polarized ultrashort electromagnetic pulse with different STCs, the spatio-temporal distribution near the focus will be distorted and degraded when it is focused by a parabolic mirror. Firstly, we describe the general formulas of the theoretical model, mainly including the Stratton-Chu's VDI and temporal discretization for a broad spectrum. Secondly, three common STC models are introduced. On this basis, the focusing characteristics of these spatio-temporal ultrashort pulses by the parabolic mirror are given respectively, via performing the full spatio-temporal distributions of electric field vectors. Then, the dependence of intensity and duration degradation of the focused field on STCs parameters is discussed. Furthermore, an ultrashort THz radiation pulse from undulator is explored to be focused to an electric field strength of 1 GV/m finally.

II. General Formula of Vector Diffraction Integral for a Parabolic Mirror

The schematic of parabolic mirror focusing is shown in Fig. 1. In a Cartesian coordinate system, the parabolic mirror is located on a paraboloidal surface, and the equation of the paraboloid is given as,

$$z = \frac{x^2 + y^2}{4f} - f, \tag{1}$$

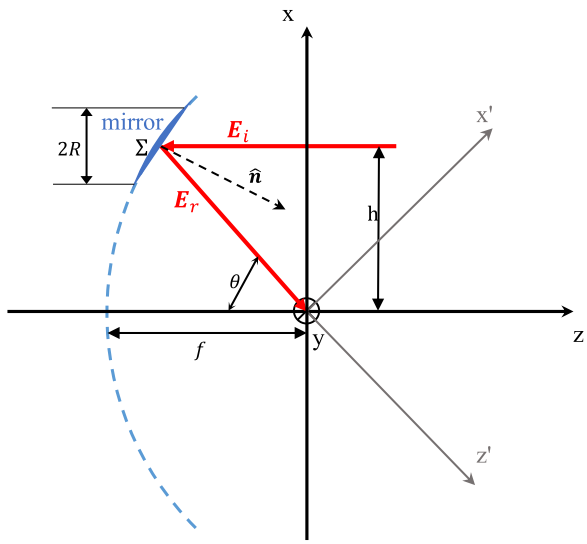

Fig. 1. Schematic of parabolic mirror focusing.

where f is the focal length, and the focus is at the origin of the coordinate system. The rotational symmetry axis of the paraboloid coincides with the z axis, and x and y are the transverse coordinates.

Then, the normal of the inner surface of the paraboloid is expressed as,

$$\mathbf{n} = \frac{1}{\sqrt{\left(1 + \frac{x^2+y^2}{4f^2}\right)}} \left(-\frac{x}{2f}\mathbf{e}_x - \frac{y}{2f}\mathbf{e}_y + \mathbf{e}_z\right), \tag{2}$$

where $\mathbf{e}_x$, $\mathbf{e}_y$ and $\mathbf{e}_z$ are basis vectors. For any circular parabolic mirror located on the paraboloid, the corresponding region Σ is specified as,

$$(x_s - h)^2 + y_s^2 \leq R^2, \tag{3}$$

where R is the transverse projection radius of the parabolic mirror, and h is the off-axis height of the parabolic mirror center from the z axis. $h = 0$ corresponds to an on-axis parabolic mirror, while $h \neq 0$ corresponds to an off-axis parabolic mirror. $S(x_s, y_s, z_s)$ represents the point on the parabolic mirror. Moreover, the area element on the paraboloidal surface can be written as,

$$dA = \sqrt{1 + \left(\frac{\partial z}{\partial x}\right)^2 + \left(\frac{\partial z}{\partial y}\right)^2}\, dxdy = \sqrt{1 + \frac{x^2 + y^2}{4f^2}}\, dxdy. \tag{4}$$

After getting these geometric distributions, we are going to discuss the focusing process of the electromagnetic field as shown in Fig. 1. First of all, it is necessary to consider the interaction process between the incident electromagnetic field and the parabolic mirror, where the electric and magnetic field are denoted as $\mathbf{E}_i$ and $\mathbf{H}_i$. After reflection, only the tangential component of the electric field and the normal component of the magnetic field change the symbol, as $\mathbf{E}_{r,t} = -\mathbf{E}_{i,t}$ and $\mathbf{H}_{r,n} = -\mathbf{H}_{i,n}$. Therefore, the reflection field is represented by

the incident field and the normal vector as,

$$\begin{aligned}\mathbf{E}_r &= 2\mathbf{n}(\mathbf{E}_i \cdot \mathbf{n}) - \mathbf{E}_i,\\ \mathbf{H}_r &= -2\mathbf{n}(\mathbf{H}_i \cdot \mathbf{n}) + \mathbf{H}_i.\end{aligned} \tag{5}$$

Next, we need to determine the diffraction field of the focal plane. According to Stratton-Chu integral formula, one can give the vector electromagnetic field in image space as [27],

$$\begin{aligned}\mathbf{E}(\mathbf{P}) = \frac{1}{4\pi}\int_{\Sigma} &[i\omega\mu_0(\mathbf{n}\times\mathbf{H})G + (\mathbf{n}\times\mathbf{E})\times\nabla G\\ &+ (\mathbf{n}\cdot\mathbf{E})\nabla G]\,dA,\\ \mathbf{H}(\mathbf{P}) = \frac{1}{4\pi}\int_{\Sigma} &[i\omega\varepsilon_0(\mathbf{E}\times\mathbf{n})G + (\mathbf{n}\times\mathbf{H})\times\nabla G\\ &+ (\mathbf{n}\cdot\mathbf{H})\nabla G]\,dA,\end{aligned} \tag{6}$$

where $\mathbf{P}(x_p, y_p, z_p)$ represents the observation point, μ_0 and ε_0 are the vacuum dielectric constant and permeability of vacuum respectively, and ω is the angular frequency of the incident field. $G(r_{sp}) = exp(ikr_{sp})/r_{sp}$, $k = \omega/c$ is the wavenumber of the electromagnetic field, and r_{sp} is the distance from a point $\mathbf{S}(x_s, y_s, z_s)$ on the parabolic mirror to a point $\mathbf{P}(x_p, y_p, z_p)$ in the image space. It needs to mention that ∇G should be calculated at the point $\mathbf{S}$ on the paraboloidal surface. In addition, the parabolic mirror discussed here is large enough to make the electromagnetic field on the mirror continuous so as to ignore contour integral [27].

The field components in the integral formula (6) are the sum of incident field and reflective field. According to (5), the total field can be expressed by incident field and normal vector as,

$$\begin{aligned}\mathbf{E}(\mathbf{S}) &= \mathbf{E}_i + \mathbf{E}_r = 2\mathbf{n}[\mathbf{n}\cdot\mathbf{E}_i(\mathbf{S})],\\ \mathbf{H}(\mathbf{S}) &= \mathbf{H}_i + \mathbf{H}_r = 2\mathbf{H}_i(\mathbf{S}) - 2\mathbf{n}[\mathbf{n}\cdot\mathbf{H}_i(\mathbf{S})].\end{aligned} \tag{7}$$

We assume a linearly polarized incident electromagnetic field with only transverse component, and it propagates along the negative z axis. Then, the monochromatic field can be expressed on the plane $\mathcal{F}$ before the parabolic mirror with dropping the time term as,

$$\begin{aligned}\mathbf{E}_{i,\mathcal{F}} &= (\mathcal{E}_x\mathbf{e}_x + \mathcal{E}_y\mathbf{e}_y)exp(-ikz),\\ \mathbf{H}_{i,\mathcal{F}} &= \sqrt{\frac{\varepsilon_0}{\mu_0}}(\mathcal{E}_y\mathbf{e}_x - \mathcal{E}_x\mathbf{e}_y)exp(-ikz).\end{aligned} \tag{8}$$

The diffraction effect of field transmission from plane $\mathcal{F}$ to parabolic mirror is ignored. After adding extra phase and setting $z = 0$ for simplicity, $\mathbf{E}_{i,\mathcal{F}}exp(-ikz_s)$ and $\mathbf{H}_{i,\mathcal{F}}exp(-ikz_s)$ can be used as the boundary conditions of the vector integral (i.e. (6)) to obtain the diffraction field in image space. Finally, the vector diffraction field is obtained by substituting (7) and (8) into (6),

$$\begin{aligned}&\mathbf{E}(\mathbf{P})\\ &= ik\frac{exp(-ikz_s)}{2\pi}\iint dx_s dy_s\\ &\times\left\{\left[\left(1-\left(1-\frac{1}{ikr_{sp}}\right)\frac{x_s(x_s-x_p)}{2fr_{sp}}\right)\mathcal{E}_x G\right.\right.\\ &\left.-\left(1-\frac{1}{ikr_{sp}}\right)\frac{y_s(x_s-x_p)}{2fr_{sp}}\mathcal{E}_y G\right]\mathbf{e}_x\\ &+\left[\left(1-\left(1-\frac{1}{ikr_{sp}}\right)\frac{y_s(y_s-y_p)}{2fr_{sp}}\right)\mathcal{E}_y G\right.\\ &\left.-\left(1-\frac{1}{ikr_{sp}}\right)\frac{x_s(y_s-y_p)}{2fr_{sp}}\mathcal{E}_x G\right]\mathbf{e}_y\\ &\left.+\left[\left(\frac{x_s}{2f}\mathcal{E}_x+\frac{y_s}{2f}\mathcal{E}_y\right)\left(1-\left(1-\frac{1}{ikr_{sp}}\right)\frac{z_s-z_p}{r_{sp}}\right)G\right]\mathbf{e}_z\right\},\\ &\mathbf{H}(\mathbf{P})\\ &= ik\sqrt{\frac{\varepsilon_0}{\mu_0}}\frac{exp(-ikz_s)}{2\pi}\iint dx_s dy_s\left(1-\frac{1}{ikr_{sp}}\right)\frac{G}{r_{sp}}\\ &\times\left\{\left[-\frac{x_s(y_s-y_p)}{2f}\mathcal{E}_x\right.\right.\\ &\left.+\left(\frac{x_s^2+y_s^2}{4f}-f-\frac{y_s(y_s-y_p)}{2f}\right)\mathcal{E}_y\right]\mathbf{e}_x\\ &+\left[\frac{y_s(x_s-x_p)}{2f}\mathcal{E}_y-\left(\frac{x_s^2+y_s^2}{4f}-f-\frac{x_s(x_s-x_p)}{2f}\right)\mathcal{E}_x\right]\mathbf{e}_y\\ &\left.+[(y_s-y_p)\mathcal{E}_x-(x_s-x_p)\mathcal{E}_y]\,\mathbf{e}_z\right\}.\end{aligned} \tag{9}$$

For off-axis case ($h \neq 0$), to facilitate the description of the reflected electromagnetic field, a more suitable new coordinate system need to be established. As shown in Fig. 1, the new coordinate system (x', y', z') is obtained by the rotation of the original coordinate system (x, y, z) along the y axis with an angle θ, which can be expressed as $tan\theta = h/(h^2/4f - f)$. In the new coordinate frame, the electromagnetic field can be given by,

$$\begin{aligned}\mathbf{E}'(\mathbf{P}) &= \mathbf{M}(\theta)\mathbf{E}(\mathbf{P}),\\ \mathbf{H}'(\mathbf{P}) &= \mathbf{M}(\theta)\mathbf{H}(\mathbf{P}),\end{aligned} \tag{10}$$

where $\mathbf{M}(\theta)$ is the rotation matrix,

$$\mathbf{M}(\theta) = \begin{pmatrix} cos\theta & 0 & sin\theta\\ 0 & 1 & 0\\ -sin\theta & 0 & cos\theta\end{pmatrix}. \tag{11}$$

The preceding discussion presents the formula for the focusing of monochromatic electromagnetic fields. For ultrashort pulses with STCs, since the tightly focusing effect is closely related to the wavelength, the influence of the broad spectrum

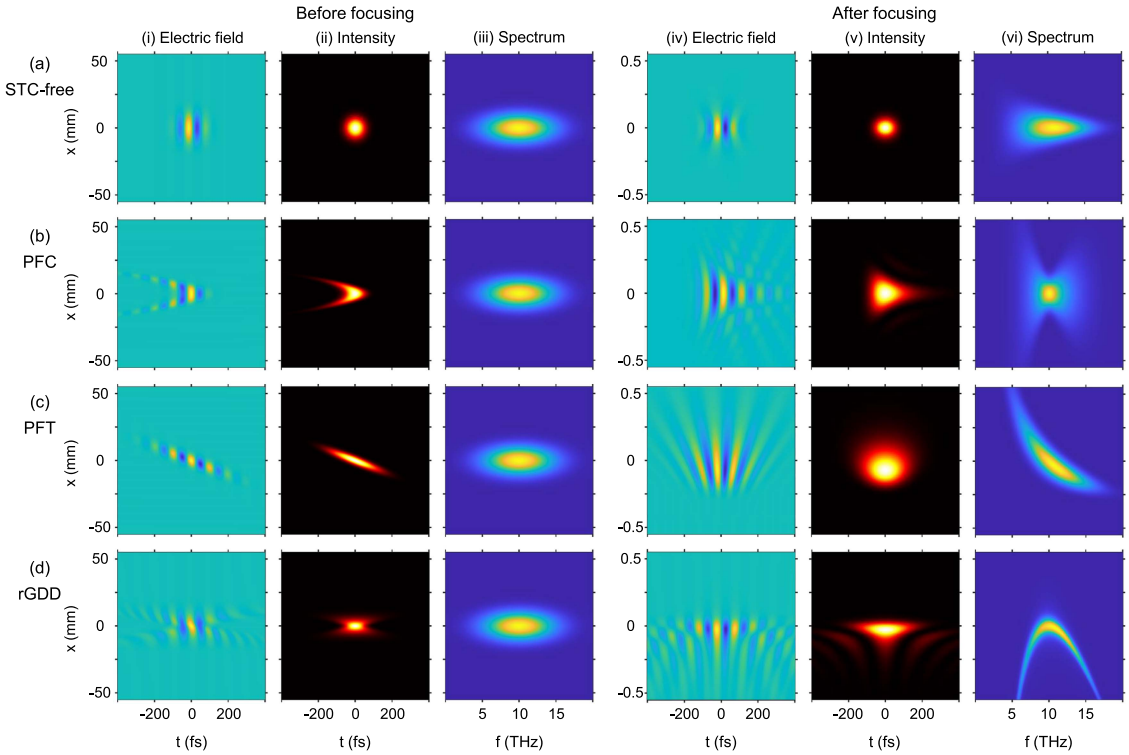

Fig. 2. Spatio-temporal characterization of the ultrashort laser before (three columns on the left) and after focusing (three columns on the right). The waveform and intensity of the electric field are given in (x, t), and the spectrums are given in (x, f): (a) Gaussian STC-free beam, (b) pulse-front curvature (PFC) beam with $\alpha = 10fs/mm^2$, (c) pulse-front tilt (PFT) beam with $\beta = 10fs/mm$, (d) beam with a radially increasing group delay dispersion (rGDD) with $\gamma = 20fs^2/mm$. The initial beam parameters: frequency $\omega_0 = 10$ THz, FWHM duration $\tau_0 = 116$ fs, waist size: $w_0 = 10$ mm. The parabolic mirror parameters: focal length: $f = 100$ mm, off-axis height: $h = 0$ m.

of ultrashort laser pulses on the focal spot must be considered. To this end, the incident electromagnetic field should be discretized in the frequency domain, while considering the spatio- and frequency-related amplitude and phase. The extension of spatial relation is to consider the spatio-temporal coupling of pulses. The electric field is given as (the magnetic field can be given by analogy),

$$\begin{aligned}\mathbf{E}_i(\mathbf{S},\omega_j) = &\left[\mathcal{E}_x(\mathbf{S},\omega_j)\mathbf{e}_x + \mathcal{E}_y(\mathbf{S},\omega_j)\mathbf{e}_y\right] \\ &\times exp\left[-i\phi(\mathbf{S},\omega_j)\right] exp(-ikz_s),\end{aligned} \tag{12}$$

where ω_j refers to the discrete frequency corresponding to the j_{th} sampling. After getting the focusing field distribution of each monochromatic field in the observation space, the final focusing field $\mathbf{E}_f$ distribution of the ultrashort pulse can be obtained by the coherent superposition, and the electric field is summed,

$$\mathbf{E}_f(\mathbf{P},t) = \sum_{j=1}^{N} \mathbf{E}_j(\mathbf{P},\omega_j) e^{-i\omega_j t} d\omega, \tag{13}$$

where $\mathbf{E}_j$ refers to the distribution after the focusing of the monochromatic field in the j_{th} sampling.

III. Spatio-Temporal Couplings and Focusing of Ultrashort THz Pulses

In this section, the effects of spatio-temporal couplings on the ultrashort pulse focusing are inspected. Compared with the spatial distribution of long pulses, which is independent of time, the spatial distribution of less periodic pulses has a time-dependence variation. In the frequency domain, an initial electric field can be expressed as $E(\mathbf{r},\omega) = \mathcal{E}_0(\mathbf{r},\omega)e^{i\phi(\mathbf{r},\omega)}$ with $\mathbf{r}$=$\mathbf{r}$(x,y) is the transverse coordinate. Here, $\mathcal{E}_0(\mathbf{r},\omega)$, $\phi(\mathbf{r},\omega)$ are spectral amplitudes and phases in different transverse spaces. Spectral phase $\phi(\mathbf{r},\omega)$ is a critical parameter determining the properties of ultrashort laser beams. To explain the key effect of this phase on an ultrashort laser beam, the Taylor expansion is performed at the center frequency ω_0,

$$\begin{aligned}\phi(\mathbf{r},\omega) = &\phi_0(\mathbf{r},\omega_0) + \phi_1(\mathbf{r},\omega_0)(\omega-\omega_0) \\ &+ \frac{\phi_2(\mathbf{r},\omega_0)}{2}(\omega-\omega_0)^2 + \cdots,\end{aligned} \tag{14}$$

where third- and higher-order terms are ignored. The first term ϕ_0 on the right side describes the phase distribution of center frequency ω_0 at different transverse positions. The second term ϕ_1 denotes the group delay of different transverse spaces, which determines the arrival time of pulses at different positions. The third term ϕ_2 describes the group delay dispersion at different positions, which can be understood as the laterally varying linear chirp.

To manifest the spatio-temporal couplings intuitively, several examples of STCs are given in Fig. 2, which displays the carrier waveform of electric field, intensity and spectrum for different couplings respectively. A Gaussian beam without STC is also described in Fig. 2(a) as a reference, and the assumed Gaussian STC-free beam before focusing has a central frequency of $f_0 = \omega_0/2\pi = 10$ THz, a duration of $\tau_0 = 116$ fs (FWHM) and a pulse waist of $w_0 = 10$ mm. In the meantime, the other STCs beams have the same parameters.

As low-order spatio-temporal couplings, pulse-front curvature (PFC) and pulse-front tilt (PFT) are the two most common STCs of ultrashort pulses. They are both related to ϕ_1 and exhibit pulse-front distortions. Let's first describe the STCs of the ultrashort pulse before focusing. Fig. 2(b)(i), (ii), (iii) shows the PFC beam, which can be characterized by a spatio-spectral phase $\phi(\mathbf{r}, \omega) = \alpha r^2(\omega - \omega_0)$, and α is the parameter representing the magnitude of PFC. Although its duration is spatially constant, the arrival time is quadratically related to the radial position. The spatio-spectral phase depends on the frequency linearly and the transverse position quadratically. Fig. 2(c)(i), (ii), (iii) shows the PFT beam, which can be described by $\phi(\mathbf{r}, \omega) = \beta x(\omega - \omega_0)$, and β is the parameter representing the magnitude of PFT. The duration of the beam is also spatially constant, but the arrival time varies linearly along the radial position. Its phase varies linearly along radial position and the corresponding slope varies linearly with frequency.

As one of the higher-order couplings, we illustrate a simple extension of the previous two couplings, where the phase is quadratically dependent on frequency. The beam exhibits a space-dependent spectral chirp. It's clearly performed in Fig. 2(d)(i), (ii), (iii) that the radially increased group delay dispersion (rGDD), which can be expressed as $\phi(\mathbf{r}, \omega) = \gamma x(\omega - \omega_0)^2$, and γ represents the magnitude of the rGDD. The phase variation is quadratic with the frequency, and it can be understood that the spectra components have a quadratically frequency-dependent wavefront tilt. Different from the low-order STCs, its local pulse length increases along the radial direction for its high-order phase modulation.

It can be found in column (i) of Fig. 2 that the carrier waveform of the electric field distorts with the space position under the STCs. These distortions correspond to the spatial variation of the phase of the electric field in the frequency domain and make the focusing effects of light fields different in the focusing space. Using the vector diffraction integral and coherent superposition methods introduced in the previous section, it can be characterized that the spatio-temporal field distribution after parabolic mirror. Whereby the numerical simulation, the ultrashort pulse focusing can be considered with arbitrary couplings.

The distributions of image space after focusing are shown in right three columns (iv,v,vi) of Fig. 2. For ultrashort pulses without STC, although the pulse length keeps constant, the focusing changes the carrier phase. This corresponds to the manifestation on the spectrum that as the radial position increases, the strength of the high-frequency component decreases. The duration of the ultrashort pulse with couplings changes significantly after focusing, and the local pulse length is different from the global pulse length distinctly. For the focused PFC beams, different frequencies of the incident field have different degrees of wavefront curvature, which makes them have different longitudinal optimal focusing positions. The duration and arrival time of the focused beam vary along the radial coordinate while the longest local pulse duration is on the propagating axis. For the focused PFT beams, the initial phase varies linearly in position with a slope that varies linearly with frequency, which leads to different transverse optimal focusing positions. The transverse chirp distribution appears on the focused spectrum and the pulse duration changes significantly. The phase of the focused electric field rotates in the opposite direction, which describes the fact that the propagation direction of the beam rotates over time within the pulse envelope (Fig. 2(c)(iv)). For the focused rGDD beam, the frequency-dependent wavefront tilt leads to a quadratic optimal focus position along the radial coordinate in the focus spot (Fig. 2(d)(vi)). This also makes the pulses form a complex spatio-temporal distribution in the transverse dimension (Fig. 2(d)(v)).

The vector characteristics of the focused field are preserved by the vector diffraction integral method. Considering a case with a 90° off-axis parabolic mirror, the time-dependent field intensities ($|E_{x'}|^2$, $|E_{y'}|^2$, $|E_{z'}|^2$) in the focal plane are shown in Fig. 3, which gives a more complete spatio-temporal presentation of the focused field. For the case of STC-free (Fig. 3(a)), the $E_{x'} = 0$ along the $y' = 0$ and the $E_{y'} = 0$ along the $x' = 0$, consistent with previous studies that don't consider STCs [31], [32]. For the pulses with different STCs, their focal spots all become larger, resulting in declining peak intensities. However, the distributions of different focused field components distort in different forms. For the PFC beam, the field components after focusing still maintain the same symmetry as the STC-free beam, but some side-lobes appear around. The same phenomenon also occurs in the focus field of rGDD beam. Although there is no side lobe in the PFT beam, it can be found that the peak intensity center has a significant lateral shift. After considering the couplings of incident ultrashort pulse, all the focusing fields present complex distributions.

The transverse electric field distribution in the focal plane is shown in Fig. 4. While obtaining the distributions of the transverse electric field waveform at the time of peak intensity, Fig. 4 also shows the intensity ratios of different field vectors. Obviously, the $E_{x'}$ component dominates the focus field, originating from the x polarization of the incident beam. The components along y' and z' are obtained under mirror reflection. Especially for the PFT beam, it will project more components to these two directions. Besides, the intensity of $E_{y'}$ and $E_{z'}$ is related to the off-axis height of the parabolic mirror.

From the above discussion, the existence of STCs will cause the attenuation of the focused ultrashort beam, which is reflected in not only the decrease of peak intensity and the increase of transverse spot size, but also the increase and distortion of focusing beam in temporal distribution. In order to further measure these effects, the changes of peak intensity and on-axis pulse duration after focusing with different STCs are given in Fig. 5 as functions of corresponding STC parameters (α, β, γ) and beam waist size w. The intensity I is normalized to the peak intensity of the corresponding incident beam. It can be

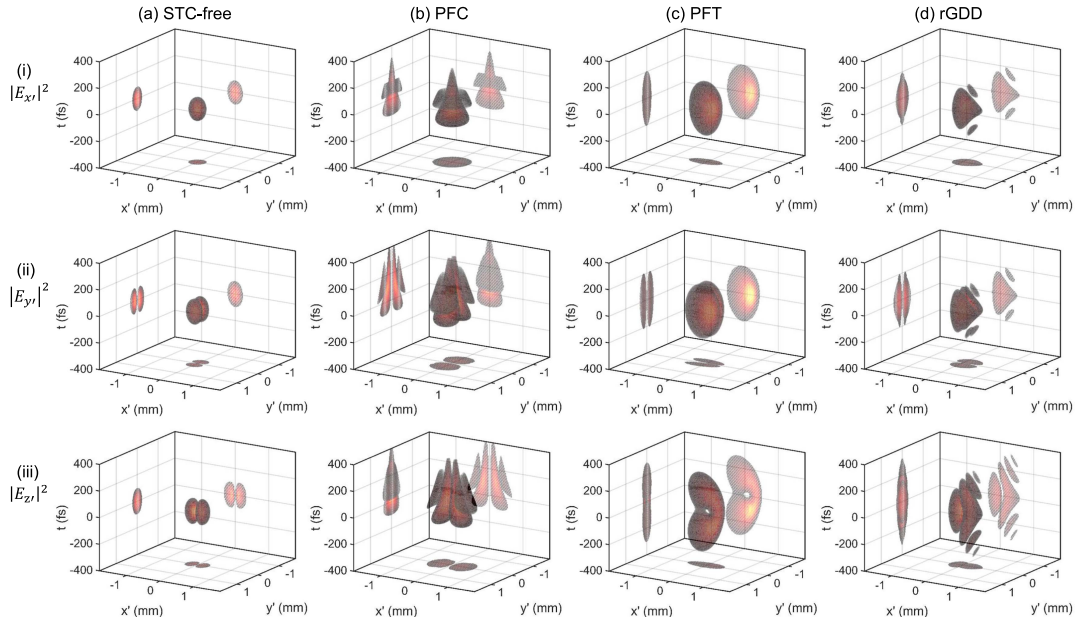

Fig. 3. Full spatio-temporal intensity distribution after 90° off-axis parabolic mirror focusing. The projections on the (x, t), (y, t) and (x, y) are also given. (a) STC-free beam, (b) PFC beam, (c) PFT beam and (d) rGDD beam. The unmentioned parameters are same with Fig. 2.

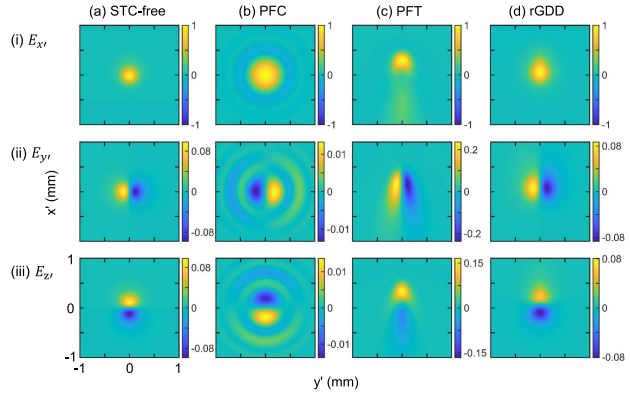

Fig. 4. Transverse distribution of the electric field in the focal spot at the time of maximal field intensity. The field components of (a) STC-free, (b) PFC, (c) PFT and (d) rGDD beams are scaled with the their maximum field strengths. The parameters used in simulation are same with Fig. 3.

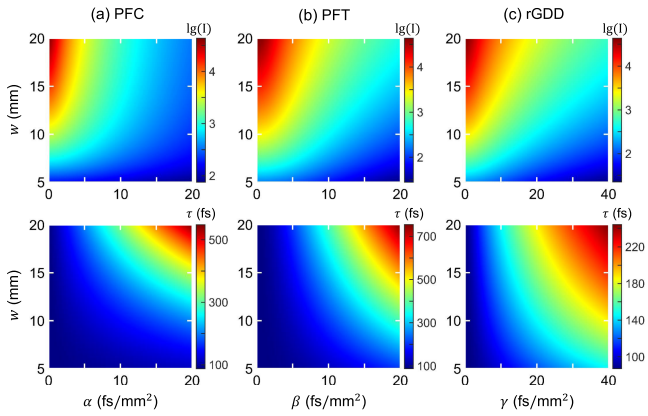

Fig. 5. Consequences of STCs at focus. The normalized peak intensity (top) and on-axis duration (bottom) verse the initial waist size and STC parameters for (a) PFC, (b) PFT and (c) rGDD beams. Other parameters are same with Fig. 3.

found that with the increase of the STCs parameters, the peak intensity of the focusing field decreases rapidly, and the pulse duration on the axis also degrades. The increase of the waist size of the initial incident beam will further aggravate the influence of STCs on the pulse duration, but it can effectively improve the normalized peak intensity. Therefore, when focusing ultrashort THz pulses through off-axis parabolic mirrors, attention should be paid to the influence of STC on the targeted properties that can be achieved by focusing, especially, when there is a strict requirement to the field strength or time length of the focused field.

IV. Focusing of an Ultrashort THz Pulses From Undulator Radiation

Since the accelerator-based THz radiation is closely related to the characteristics of the electron beam, THz pulses with tunable frequency and high power can be obtained by modulating the electron beam. In previous studies [33], [34], an ultrashort strong-field THz radiation can be obtained by the modulated electron beam and matched undulator. The peak electric field can reach 60 MV/m with quasi sub-cycle oscillation as the gray line shown in Fig. 6(a). To further expend such an ultrashort THz pulse to science applications that require more intense THz electromagnetic fields, parabolic mirror focusing can be considered as an excellent method to improve its electric field strength. However, this THz beam has a complex wavefront distribution, which may hinder the improvement of the focused field strength and even destroy its temporal waveform. So it's necessary to measure its performance under focusing. Using the aforementioned simulation method, the focusing results of this spatio-temporal ultrashort THz beam are discussed in the following.

The initial pulse distribution is shown in Fig. 6(a) and (b). This is a rotationally symmetric ultrashort THz pulse whose

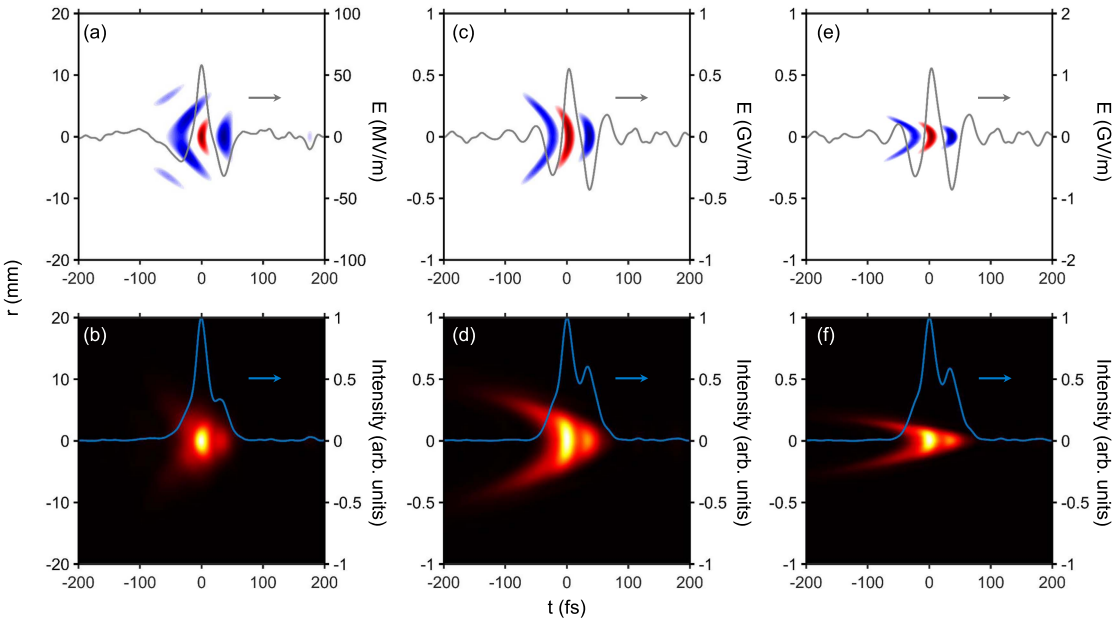

Fig. 6. Spatio-temporal characterizations of the electric field (upper) and intensity (bottom) of the ultrashort THz radiation pulse from undulator (a) initially, (b)after focusing and (c) after focusing with doubled waist. The gray and blue lines represent the on-axis electric field and intensity respectively.

polarization state is linear polarization along the x-axis. Under the focusing effect of a 90° off-axis parabolic mirror with a focal length of 5 cm, its spatial and temporal distributions on the focusing plane are shown in Fig. 6(c) and (d). One can see that the lateral beam size is compressed below 1 mm and the peak intensity increased from 60 MV/m to 600 MV/m. After focusing, the pulse distribution shows characteristic similar to the PFC beam. The pulse duration of the focused beam has increased distinctly. As the blue line is shown in Fig. 6, the time length on the axis has declined and distorted, especially the appearance of another intensity peak outside the main peak. In order to further improve the focusing field strength, it assumes that the waist of the incident beam is doubled without other changes. Then, the focused field is shown in Fig. 6(e) and (f) that the time structure doesn't change significantly but the electric field strength increases to 1 GV/m.

V. Conclusion

In this paper, we present the characterization of parabolic mirror focusing of ultrashort THz pulses with spatio-temporal couplings. For several common STC models, the complete vector distribution of electromagnetic field in the focusing space is obtained based on vector diffraction integral. To deal with the ultrashort pulse with a wide spectrum, the incident electric field is discretized in the frequency domain, and then the diffraction fields of each component superimpose on the focal plane. The numerical results show that STCs cause the degradation of the focused field, which is specifically manifested in reducing the field intensity and distorting the pulse time structure. However, the incident pulse with a large waist can decrease the influence of STCs on the focused field intensity. Besides, we give a discussion about the possibility to improve the electric field of an ultrashort THz pulse from undulator to 1 GV/m. The method described in this paper also applies to other frequencies, especially for the ultraintense optical laser community.

References

[1] T. Kampfrath, K. Tanaka, and K. Nelson, "Resonant and nonresonant control over matter and light by intense terahertz transients," *Nature Photon.*, vol. 7, no. 9, pp. 680–690, 2013.
[2] P. Salén et al., "Matter manipulation with extreme terahertz light: Progress in the enabling THz technology," *Phys. Rep.*, vol. 836/837, pp. 1–74, 2019.
[3] M. Kozina et al., "Terahertz-driven phonon upconversion in $SrTiO_3$," *Nature Phys.*, vol. 15, no. 4, pp. 387–392, 2019.
[4] R. Matsunaga et al., "Light-induced collective pseudospin precession resonating with Higgs mode in a superconductor," *Science*, vol. 345, no. 6201, pp. 1145–1149, 2014.
[5] F. Chen et al., "Ultrafast terahertz-field-driven ionic response in ferroelectric $BaTiO_3$," *Phys. Rev. B*, vol. 94, no. 18, 2016, Art. no. 180104.
[6] B. Zaks, R. Liu, and M. Sherwin, "Experimental observation of electron-hole recollisions," *Nature*, vol. 483, no. 7391, pp. 580–583, 2012.
[7] M. Liu et al., "Terahertz-field-induced insulator-to-metal transition in vanadium dioxide metamaterial," *Nature*, vol. 487, no. 7407, pp. 345–348, 2012.
[8] S. Winnerl et al., "Carrier relaxation in epitaxial graphene photoexcited near the Dirac point," *Phys. Rev. Lett.*, vol. 107, no. 23, 2011, Art. no. 237401.
[9] K. Grishunin et al., "Terahertz magnon-polaritons in $TmFeO_3$," *ACS Photon.*, vol. 5, no. 4, pp. 1375–1380, 2018.
[10] T. Kampfrath et al., "Coherent terahertz control of antiferromagnetic spin waves," *Nature Photon.*, vol. 5, no. 1, pp. 31–34, 2011.
[11] S. Bonetti et al., "THz-driven ultrafast spin-lattice scattering in amorphous metallic ferromagnets," *Phys. Rev. Lett.*, vol. 117, no. 8, 2016, Art. no. 087205.
[12] S. Fleischer, R. Field, and K. Nelson, "Commensurate two-quantum coherences induced by time-delayed THz fields," *Phys. Rev. Lett.*, vol. 109, no. 12, 2012, Art. no. 123603.
[13] J. Larue et al., "THz-pulse-induced selective catalytic CO oxidation on Ru," *Phys. Rev. Lett.*, vol. 115, no. 3, 2015, Art. no. 036103.
[14] H. Xu et al., "Cascaded high-gradient terahertz-driven acceleration of relativistic electron beams," *Nature Photon.*, vol. 15, no. 6, pp. 426–430, 2021.

[15] L. Zhao et al., "Terahertz oscilloscope for recording time information of ultrashort electron beams," *Phys. Rev. Lett.*, vol. 122, no. 14, 2019, Art. no. 144801.
[16] Z. Tibai, S. Turnár, G. Tóth, J. Hebling, and S. W. Jolly, "Spatiotemporal modeling of direct acceleration with high-field terahertz pulses," *Opt. Exp.*, vol. 30, no. 18, pp. 32861–32870, 2022.
[17] S. Akturk, X. Gu, P. Bowlan, and R. Trebino, "Spatio-temporal couplings in ultrashort laser pulses," *J. Opt.*, vol. 12, no. 9, 2010, Art. no. 093001.
[18] A. April, "Ultrashort, strongly focused laser pulses in free space," in *Coherence and Ultrashort Pulse Laser Emission*. Rijeka, Croatia: IntechOpen, 2010, pp. 355–382.
[19] J.-X. Li, Y. Salamin, K. Hatsagortsyan, and C. Keitel, "Fields of an ultrashort tightly focused laser pulse," *J. Opt. Soc. Amer. B*, vol. 33, no. 3, pp. 405–411, 2016.
[20] V. Fedorov, M. Chanal, D. Grojo, and S. Tzortzakis, "Accessing extreme spatiotemporal localization of high-power laser radiation through transformation optics and scalar wave equations," *Phys. Rev. Lett.*, vol. 117, no. 4, 2016, Art. no. 043902.
[21] A. Couairon et al., "Propagation equation for tight-focusing by a parabolic mirror," *Opt. Exp.*, vol. 23, no. 24, pp. 31240–31252, 2015.
[22] D. Shipilo et al., "Tight focusing of electromagnetic fields by large-aperture mirrors," *Phys. Rev. E*, vol. 100, no. 3, 2019, Art. no. 033316.
[23] V. S. Ignatovsky, "The relationship between geometric and wave optics and diffraction of an azimuthally symmetric beam," *Trans. Opt. Inst. Petrograd*, vol. 1, 1920, Art. no. 3.
[24] J. Stratton and L. Chu, "Diffraction theory of electromagnetic waves," *Phys. Rev.*, vol. 56, no. 1, pp. 99–107, 1939.
[25] E. Wolf, "Electromagnetic diffraction in optical systems - I. An integral representation of the image field," *Proc. Roy. Soc. London Ser. A. Math. Phys. Sci.*, vol. 253, no. 1274, pp. 349–357, 1959.
[26] B. Richards and E. Wolf, "Electromagnetic diffraction in optical systems, II. structure of the image field in an aplanatic system," *Proc. Roy. Soc. London Ser. A. Math. Phys. Sci.*, vol. 253, no. 1274, pp. 358–379, 1959.
[27] P. Varga and P. Török, "Focusing of electromagnetic waves by paraboloid mirrors. I. theory," *J. Opt. Soc. Amer. A: Opt. Image Sci., Vis.*, vol. 17, no. 11, pp. 2081–2089, 2000.
[28] P. Varga and P. Török, "Focusing of electromagnetic waves by paraboloid mirrors. II. numerical results," *J. Opt. Soc. Amer. A*, vol. 17, no. 11, pp. 2090–2095, 2000.
[29] S.-W. Bahk et al., "Characterization of focal field formed by a large numerical aperture paraboloidal mirror and generation of ultra-high intensity (1022 w/cm2)," *Appl. Phys. B: Lasers Opt.*, vol. 80, no. 7, pp. 823–832, 2005.
[30] X. Zeng and X. Chen, "Characterization of tightly focused vector fields formed by off-axis parabolic mirror," *Opt. Exp.*, vol. 27, no. 2, pp. 1179–1198, 2019.
[31] T. Jeong, S. Weber, B. Le Garrec, D. Margarone, T. Mocek, and G. Korn, "Spatio-temporal modification of femtosecond focal spot under tight focusing condition," *Opt. Exp.*, vol. 23, no. 9, pp. 11641–11656, 2015.
[32] J. Dumont, F. Fillion-Gourdeau, C. Lefebvre, D. Gagnon, and S. Maclean, "Efficiently parallelized modeling of tightly focused, large bandwidth laser pulses," *J. Opt.*, vol. 19, no. 2, 2017, Art. no. 025604.
[33] H. Zhang et al., "Generation of frequency-chirped density modulation electron beam for producing ultrashort THz radiation pulse," *Phys. Rev. Accel. Beams*, vol. 23, no. 2, 2020, Art. no. 020704.
[34] H. Zhang et al., "Tuning electron bunch with a longitudinally shaped laser to generate half-cycle terahertz radiation pulse," *J. Instrum.*, vol. 16, no. 8, 2021, Art. no. P08019.